High-Temperature Solid Particle Erosion Behavior of Partially Oxidized NiCrBSiFe/NiCr Plasma Spray Coatings

Subba Rao Medabalimi[1] · M. R. Ramesh[1] · Ravikiran Kadoli[1]

Abstract This paper investigated the solid particle erosion behavior of partially oxidized NiCrBSiFe and NiCr coatings by varying temperature and impact angle. The challenge in the current situation is to process a new system of powders containing metallic and oxide phases. Partially oxidized powders containing metallic and oxide phases were processed by flame spraying the alloy powders into distilled water and allowing the oxide layer to form while keeping the core in the middle of the particle. Partially oxidized coatings were developed on MDN321 steel using the plasma spray technique with feedstock of partially oxidized powders. An air jet erosion test was carried out using Al_2O_3 erodent of grit size 50 μm at room temperature, 200, 400, 600, and 800°C by varying 30, 45, 60, 75, and 90° impact angles. Coatings were characterized concerning bond strength, porosity, micro-hardness, and density. The effect of temperature and impact angle on volumetric erosion loss was studied using SEM, EDS, and XRD analysis. Partially oxidized NiCrBSiFe coating exhibited better erosion resistance compare with partially oxidized NiCr coating. NiCr coating demonstrates maximum volumetric erosion loss at 45° impact angle, whereas NiCrBSiFe at 60° impact angle under all tested temperatures.

Keywords bond coat · flame spray · high-temperature erosion · mixed-mode of erosion · oxide layer · partial oxidization · plasma spray

✉ Subba Rao Medabalimi
  msr1904@gmail.com

1 Department of Mechanical Engineering, National Institute of Technology Karnataka, Surathkal, Mangalore 575025, India

Introduction

One major issue to study the degradation of material in tribological concern is solid particle erosion, which is defined as the gradual removal of material from the targeted surface by continuous impact with the solid particle (Ref 1, 2). Its severity increases at high temperatures like in jet engine parts, gas turbine blades, coal-fired thermal power plants, boiler tubes, etc. (Ref 3-6). In such a case, the erosion resistance of the components can be improved by surface modification techniques. Thermal spray coatings, reinforcement by the oxide phases, and heat treatment of the surfaces are solutions to improve the resistance to surface degradation (Ref 7-9). Plasma spray is an extensively used thermal spray process for the deposition of metallic and non-metallic materials to enhance the erosion resistance of an industrial component (Ref 10). The oxide coatings developed by the plasma spray process are widely used to improve wear, erosion, corrosion, and oxidation resistance (Ref 11, 12, 13). On the other side, pure oxide coatings are not suggested for improving erosion resistance due to their high brittleness (Ref 14). However, combing oxide phases with a metallic matrix optimizes the brittleness and toughness of the coating. Nithin et al. (Ref 15) described that erosion resistance had improved by the plasma sprayed Co-based composite coating with the addition of CeO_2 and Al_2O_3. The addition of 20–40% of the oxide phase increases the coating's mechanical and tribological properties (Ref 16). The addition of pure oxide phases will improve the porosity and high-stress concentration (Ref 17). However, it is costly to process the oxides from the alloy powders by gas atomization process and difficult to attain homogeneity of the powder mixture. In addition, pure oxide coatings possess lower bond strength,

and it required a bond coat at the interface to avoid catastrophic failure of the coating during sliding wear.

To improve the toughness of oxide coatings and to reduce the cost, partially oxidized powders were processed from the alloy powders by flame spray process. When the alloy powders are sprayed into the distilled water by flame spray process, a thin oxide layer is formed around the powder particles by retaining the toughness at the core of the particle. As a result, partially oxidized powder exhibits a combined effect of hardness and toughness, which is vital to withstand erosion during impact (Ref 18). The core of partially oxidized powder acts as a binder to improve the adhesion strength during coating deposition by plasma spray. Significant bond strength of the coatings was expected even in the absence of a bond coat. Since there was no need for a bond coat and the oxides were processed directly from the alloy powders, the deposition cost of partially oxidized coatings was lower than the oxide coatings. The partially oxidized powders can be made with any alloy powder, whose elements are sensitive to oxidation (Ref 19), having ductility to make a bond with the substrate (Ref 20, 21, 22) and suitable dilatometer properties (Ref 23).

In this paper, partially oxidized powders were processed by the flame spray process from the alloy powders of NiCrBSiFe and NiCr. The partially oxidized powders were deposited on MDN321 steel without the use of a bond coat by the plasma spray process. The coating deposition cost was reduced due to the exclusion of the bond coat. Partially oxidized NiCrBSiFe and NiCr coatings were also possessed significant bond strength without a bond coat. The coatings were characterized by bond strength, porosity, micro-hardness, and density. The erosion behavior of coatings was studied using an air-jet erosion tester at RT, 200, 400, 600, and 800 °C with 30, 45, 60, 75, and 90° impact angles. Erosion loss was calculated by the weight-loss method.

Materials and Methods

Materials

NiCrBSiFe and NiCr alloy powders are sprayed using the flame spray process onto the distilled water filled in a steel tub (Fig. 1). The flame spray gun, while spraying, reciprocated linearly within the length of the tub at a constant velocity (1 m/s) to avoid bonding between the particles. Semi-solid state powder particles will undergo partial oxidation when it reaches the water. In a furnace, the wet partially oxidized powder was dried at 100°C. The powder particles were ball milled for 10 minutes to break the local welding between the particles and reduce the particle's size, followed by sieving to 50 μm (Ref 24, 25). The
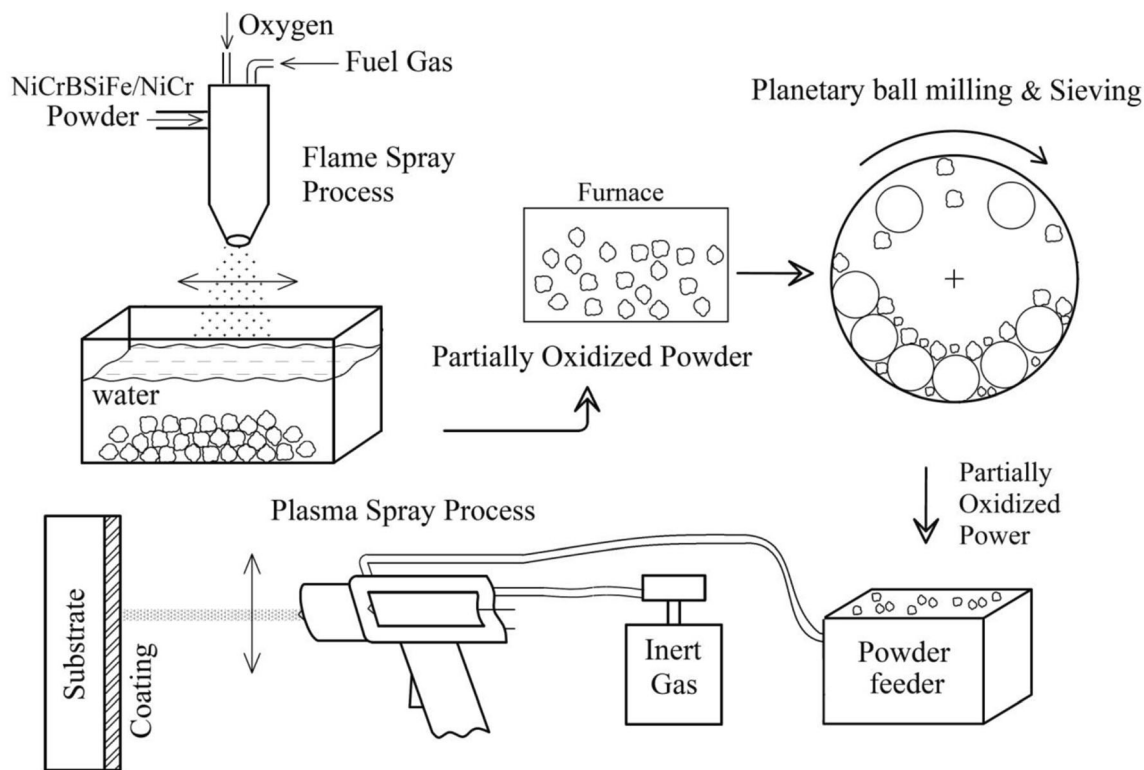

Fig. 1 Process of preparation of partially oxidized powders and deposition of the coatings

Table 1 Elemental composition of alloy powders and substrate (wt.%)

Elements	Cr	Si	Fe	B	Ti	C	Co	Ni
NiCrBSiFe	15.3	4.8	4.2	3.1	…	0.6	0.03	71.97
NiCr	20	…	…	…	…	…	…	80

Table 2 Flame spray process parameters

Air	0.6 MPa
O$_2$	6 MPa
Dissolved acetylene	5 MPa
Standoff distance	120-150 mm

Table 3 Plasma spray process parameters

Plasma gas	H$_2$ and Argon
Hydrogen	Flow 7 L/min Pressure 0.35 MPa
Argon	Flow 40 L/min Pressure 0.7 MPa
Powder feed	60 g/min
Standoff distance	100-125 mm
Arc voltage	60 V
Arc current	490 A

Table 4 Parameters used for air jet erosion tester

Erodent material	Alumina
Erodent velocity, m/s	35
Erodent average size, μm	50
Erodent feed rate, g/min	2
Temperature, °C	RT, 200, 400, 600, 800
Impact angle, °	30, 45, 60, 75 and 90
Cycle test time, min	15
Nozzle diameter, mm	1.5
Standoff distance, mm	10

elemental compositions of the alloy powders are listed in Table 1. Table 2 list the parameters used for the flame spray process.

Deposition of Coatings

Plasma spray METCO USA, 3MB equipment, was used to deposit the coatings with the feedstock of partially oxidized NiCrBSiFe and NiCr powders (Fig. 1). Parameters used for plasma spraying are mentioned in Table 3. The MDN321 steel specimens were grid blasted using alumina particles to prepare the surface suitable for the deposition of the coating. Mahantayya et al. (Ref 26) used MDN321 steel substrate for erosion studies. No bond coat was used at the coating and substrate interface. Un-oxidized NiCr content in partially oxidized powders contributes to the better bond strength of the coating. The average coating thickness is 250 μm.

Characterization

A pullout test was used to measure the bond strength of the coating as per ASTM C633-13 standard. The coated samples (25 × 25 × 5 mm) are joined on their wider faces with uncoated counter blocks (φ25 mm × 60 mm) by epoxy adhesive (DP460). Joined samples are cured 24 hours at room temperature prior to the pullout test. Shimadzu hydraulic tensile testing machine (AG-X plus) with 0.016 mm/min strain rate was used to pull the specimens. The porosity was measured along the cross-section of the coating using an inverted optical microscope (Zeiss Axiovert 200 MAT) attached with image analyzer software, as stated by ASTM B276. Twenty images are considered at 500× magnification to measure the porosity on the cross-

section. The average porosity of both the coatings was found to be less than 1.5%.

Omni-tech Vickers tester (MVH-S-AUTO) was used to measure the micro-hardness of the coating along the cross-section. Five readings were taken at every 50 μm distance from the interface under loads of 300 grams with 10 seconds dwell time. The Pycnometer was used to measure the density of the coating, as stated by ASTM C-135-96. Partially oxidized powders were cold mounted with acrylic powder and resin. The cold-mounted powders were polished with a series of SiC papers ranging from 800 to 2000 grit and then polished with diamond paste on a velvet cloth. Optical micrograph images are obtained with the help of an inverted optical microscope (Zeiss Axiovert 200 MAT) and Axio Vision SE64 software to analyze the various phases at the cross-section of partially oxidized powders.

Erosion Test

Erosion tests were carried out using an air-jet erosion tester (TR-471-800, Ducom Instruments Pvt Ltd, India) as per ASTM G76-13. The parameters used for the air jet erosion tester were listed in Table 4. Al$_2$O$_3$ particles with an average grit size of 50 μm were used as erodent (Fig. 2). The erodent was feed into the mixing chamber at 2 g/min
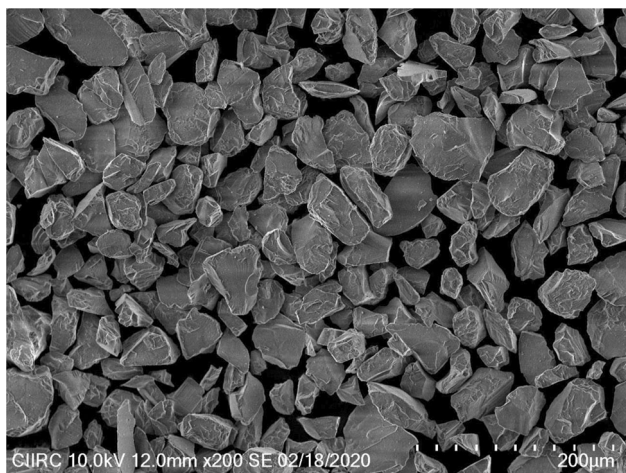
Fig. 2 SEM of Al_2O_3 erodent particles

velocity along with hot airflow. A tubular chamber surrounded the specimen holder setup with heating coils. The double-disc velocity method was used to set the erodent velocity of 35 m/s. The specimens with dimensions 25 mm × 20 mm × 5 mm were used for the 30° impact angle, while the specimens with dimensions 25 mm × 25 mm × 5 mm were used for the other impact angles.

Figure 3 shows a graphical representation of an air-jet erosion tester eroding the specimen with varying impact angles. Specimen holders for various impact angles were designed in such a way that the standoff distance between the erodent nozzle and its impact on the specimen is always maintained constant at 10 mm. The specimen holder has a hole in the bottom where a thermocouple can be placed to measure the specimen's temperature. The impingement angles of 30°, 45°, 60°, 75°, and 90° were selected to

provide the maximum erosion condition for both the ductile and brittle materials under alumina erodent. The maximum operating temperature of NiCrBSiFe/NiCr coatings is 820°C. Hence Maximum erosion testing temperature of 800°C is chosen in the present study. The erosion behavior of coating at a wide range of temperatures has been evaluated. The sample was clamped into the specimen holder with the required impact angle and heated about 20 minutes prior to the test. Each sample was eroded continuously for 15 minutes at a constant temperature. The ratio between the weight losses of the eroded sample to the coating density (ρ) is calculated as volumetric erosion loss. Each test parameter was repeated three times, and the average value was reported. A non-contact 3D optical profilometer (Zeta instrument, 20 USA) was used to quantify the volumetric erosion loss of eroded samples (Ref 17, 27).

Results and Discussion

Microstructural Characterization

The microstructural change caused due to phase transformation of powders was reflected in the properties of the coatings. XRD patterns of as-received powder, partially oxidized powder, and as-sprayed coatings depict the transformed phases at different stages of coating deposition (Fig. 4). XRD of NiCrBSiFe alloy powder reveals the formation of $FeNi_3$ phase as a higher intensity peak and CrB as a lower intensity peak. Wolfgang et al. (Ref 28) reported that NiCrBSiFe alloy powder mainly consists of $FeNi_3$, Fe_3Ni_3B, and $B(Fe, Si)_3$ phases. XRD pattern of
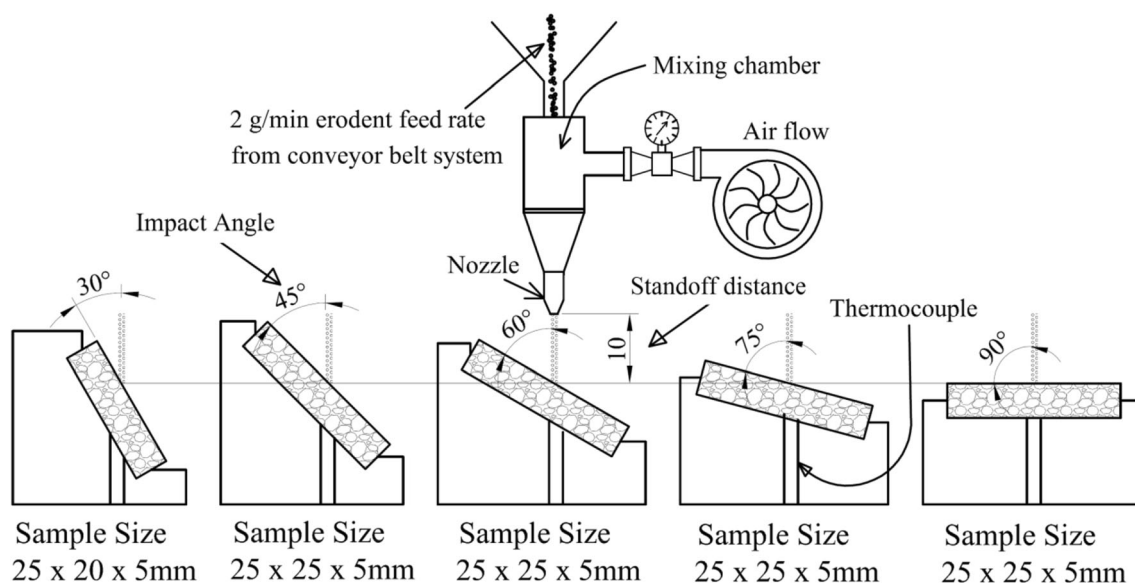

Fig. 3 Schematic representation of erodent from nozzle impacting the specimen at different angles
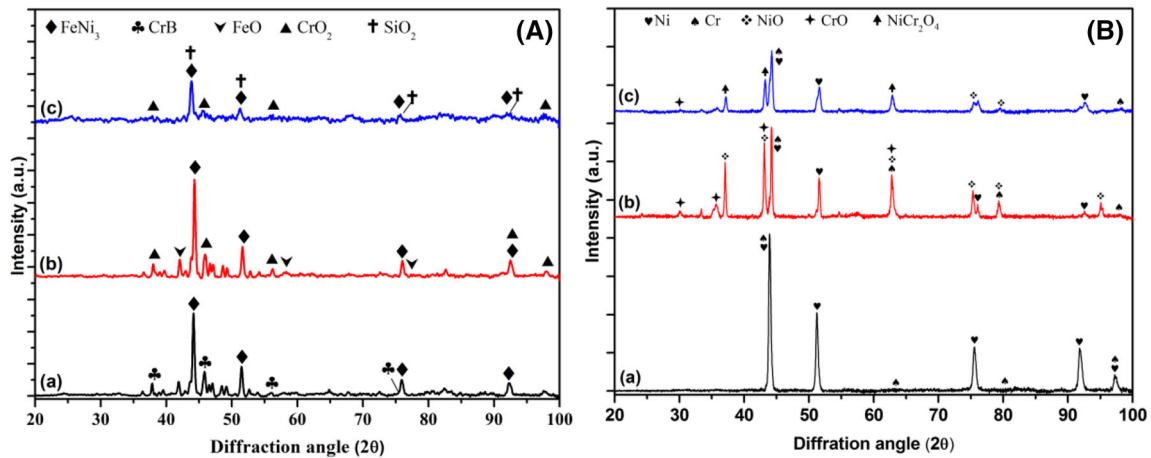
Fig. 4 XRD patterns of (A) NiCrBSiFe and (B) NiCr (a) as-received powder (b) partially oxidized powder and (c) as-sprayed coating
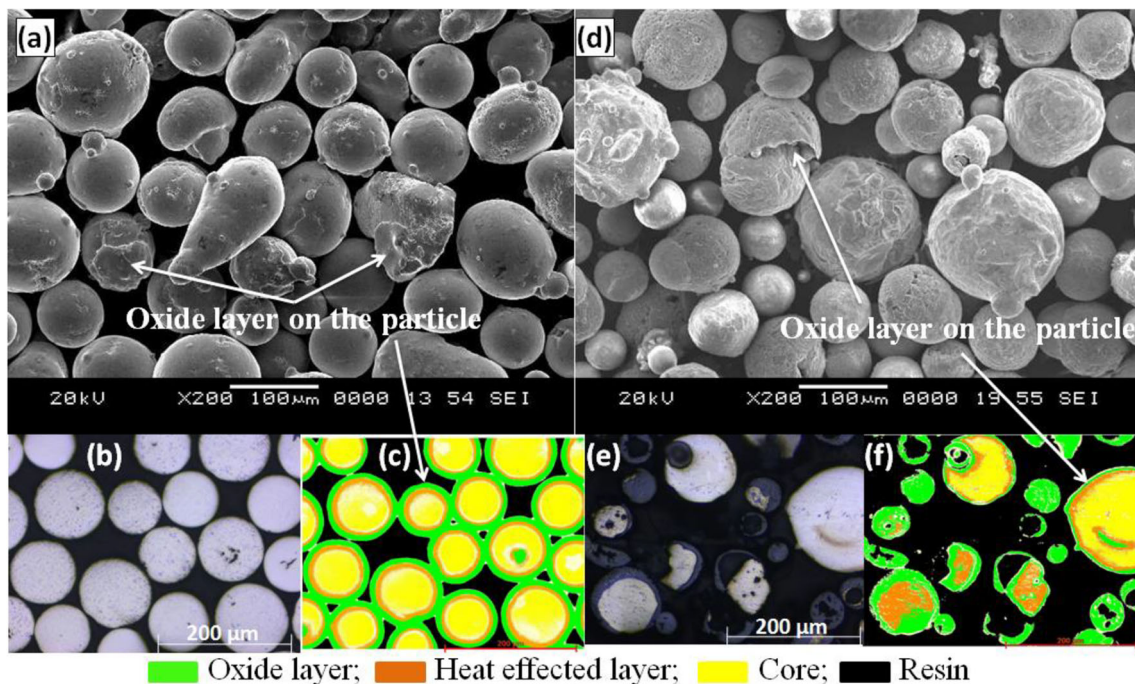

Fig. 5 NiCrBSiFe and NiCr partially oxidized powders of (a, d) SEM, (b, e) optical micrograph at the cross-section of the powders, and (c, f) metallurgical phase analyzed the image of (b, e) respectively

NiCr alloy powder describes a face-centered cubic structure with pure Ni element. Lesser intensity peaks of Cr with body-centered cubic structure presented in XRD pattern because Cr elements were dissolved with Ni. Farahpour et al. [29] noticed a similar XRD pattern of NiCr alloy powder. It is important to note that Cr elements, after partial oxidation produced chromium oxides along with nickel oxides.

During the partial oxidization process, alloy powder travels from the high-temperature flame to room temperature water. In a small duration of time, powder particles turn to a semi-solid state and are followed by sudden

cooling. Figure 5 depicts partially oxidized powders and their cross-section with an oxide layer and heat-affected layer on the core. NiCr particles can be divided into fully oxidized and partially oxidized particles based on the diameter of the particle. Smaller size particles turn semi-solid till the center and transform to full oxides, whereas larger diameter particles resist heat and form a thin oxide layer on the core. Heat-affected layer is present between the oxide layer and core for the large diameter particles. The particle size distribution of partially oxidized powders was measured using a wet dispersion process by a laser diffraction particle distribution analyzer, and the results are
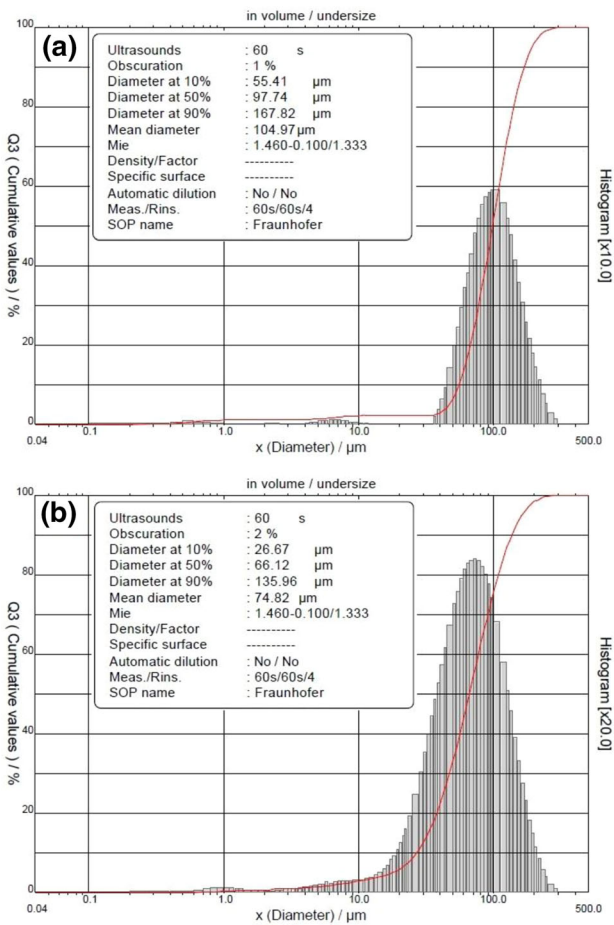
Fig. 6 Particle size distribution of (a) NiCrBSiFe (b) NiCr partially oxidized powders

shown in Fig. 6. Partially oxidized powder consists of NiO and Cr-O oxide phases, whereas coating offers spinal oxide phase $NiCr_2O_4$. During deposition of the coating by plasma spray process, partially oxidized particles produced lamellar structure. Figure 7 depicts the cross-section, surface morphology of partially oxidized NiCr coating with selected points EDS analysis and X-ray elemental mapping.

Point 5 represent the center of the partially oxidized splat and elemental percentages at point 3, 4, and 5 demonstrate an increasing percentage of oxygen as moving away from the center. 21% of oxygen at the center of point 6 represents an oxidized splat. The coating consists of partially oxidized splats overlapped by oxidized splats. Oxidized splats possess higher hardness, whereas partially oxidized splats have high toughness. This combination was the predominant requirement in the industry to increase the wear and erosion resistance of the coatings at high temperatures. X-ray elemental mapping showing the uniform distribution of Ni and Cr elements across the thickness of the coating. Elemental overlay showing the overall

percentage of oxygen is 16, which conforms oxidized regions is more than the partially oxidized region in the coating. Huang et al. (Ref 30, 31) prepared $NiCr/Cr_3C_2$ and $NiCr/BaF_2·CaF_2$ composite powders with pressurized hydrogen reduction and solid-state alloying processes. The oxide layer formed on the core contributed to better friction and wear resistance of the coating during sliding. During sliding, the oxide layer produced on the core contributed to improve friction and wear resistance of the coating.

NiCrBSiFe particle during partial oxidation produced uniform thickness of oxide layer and heat-affected layer on the core irrespective of the size of the particle. The oxide layer is thin and possesses brittle nature, whereas the core remains as ductile. Few oxide phases like FeO, CrO_2 were identified in partially oxidized powder due to a thin oxide layer on the core. XRD may not be able to detect all the oxide phases present in this thin oxide layer. SiO_2 oxide phase was formed along with $FeNi_3$ phase as a strong intensity peak in the as-sprayed coating. Figure 8(A) illustrates various elementals presented at the cross-section of partially oxidized NiCrBSiFe coatings. Points 3, 5, and 6 represent partially oxidized splats, and points 4 and 7 represent oxidized splats. The presence of a higher amount of oxygen at point 4 indicates the coating has oxidized along the splat boundaries. Uniform distribution of oxygen and elemental overlay showing six percentage of oxygen, demonstrating coating contains more partially oxidized region than the oxidized region. The minimum percentage of Ni at the interface (point 2) represents the inter-diffusion of iron from MDN321 steel.

Bond Strength

Partially oxidized coatings were developed directly on the substrate without a bond coat. The bond strength test was carried out to demonstrate the increased bond strength even in the absence of bond coat. Moreover, the durability of the coating depends on the bond strength between the coating and substrate (Ref 32). The bond strength of the coatings was determined as the ratio of the greatest load (at which the coating peeled off) to the cross-sectional area. Bond coat between substrate and coating influences the performance and properties of the plasma sprayed coatings. In thermal spray coatings, strong metallurgical self-bonding is more important between substrate and coating interface to get better performance (Ref 33). Therefore, a partially oxidized coating is deposited on the MDN321 steel specimen without a bond coat. The average adhesion strengths of NiCrBSiFe and NiCr coatings are found as 12.92 and 10.88 MPa, respectively. The researchers reported similar bond strength values with NiCr bond coat and oxide layer topcoat (Ref 20, 32).
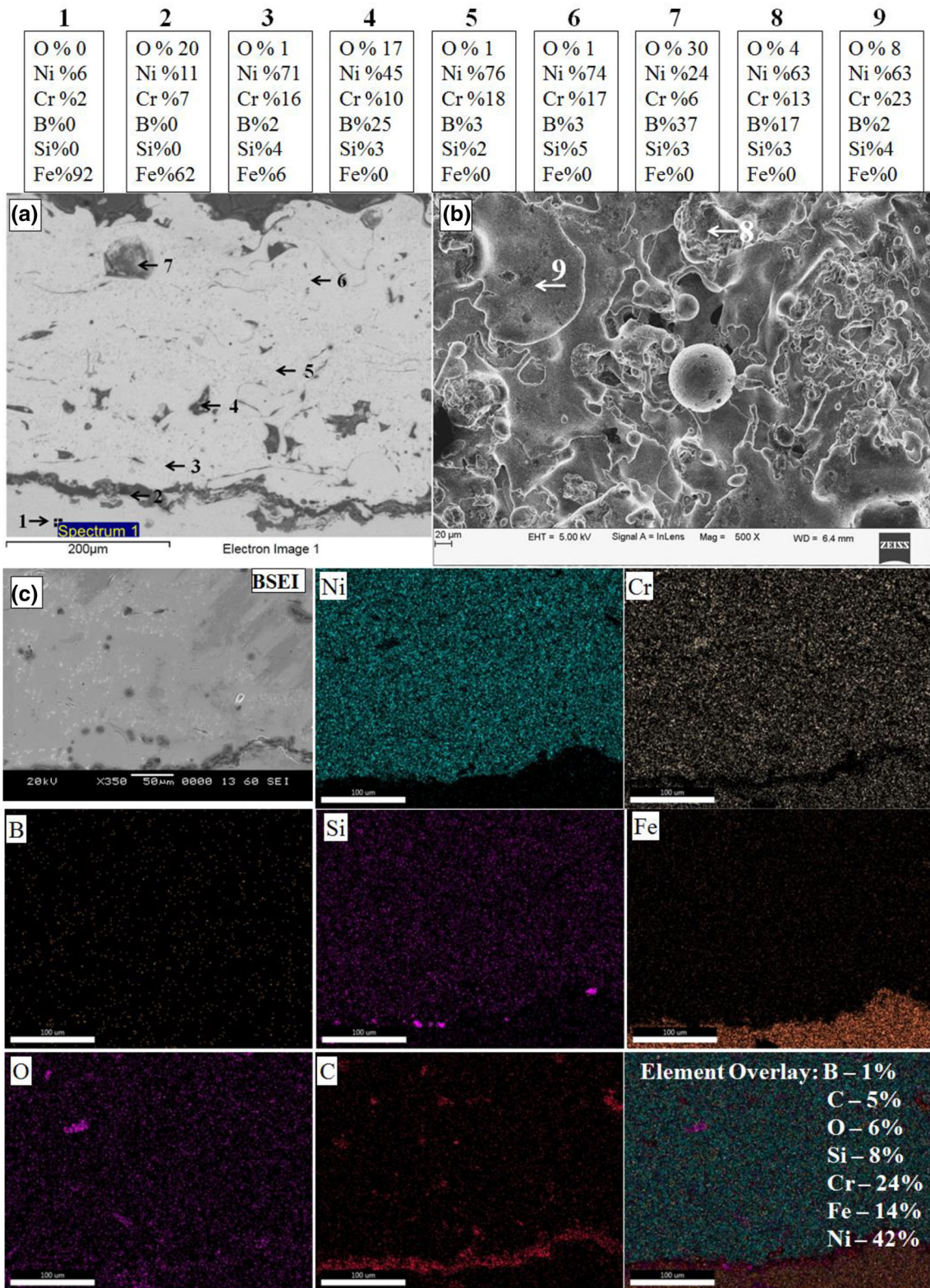
1	2	3	4	5	6	7	8	9
O % 0	O % 20	O % 1	O % 17	O % 1	O % 1	O % 30	O % 4	O % 8
Ni %6	Ni %11	Ni %71	Ni %45	Ni %76	Ni %74	Ni %24	Ni %63	Ni %63
Cr %2	Cr %7	Cr %16	Cr %10	Cr %18	Cr %17	Cr %6	Cr %13	Cr %23
B%0	B%0	B%2	B%25	B%3	B%3	B%37	B%17	B%2
Si%0	Si%0	Si%4	Si%3	Si%2	Si%5	Si%3	Si%3	Si%4
Fe%92	Fe%62	Fe%6	Fe%0	Fe%0	Fe%0	Fe%0	Fe%0	Fe%0

Fig. 7 NiCrBSiFe partially oxidized coating demonstrating (a) BSEI with EDS analysis at selected points on the cross-section (b) surface morphology showing partially melted and melted splats with EDS point analysis (c) X-ray elemental mapping with BSEI and element overlay at the cross-section of as-sprayed coating on MDN321 steel
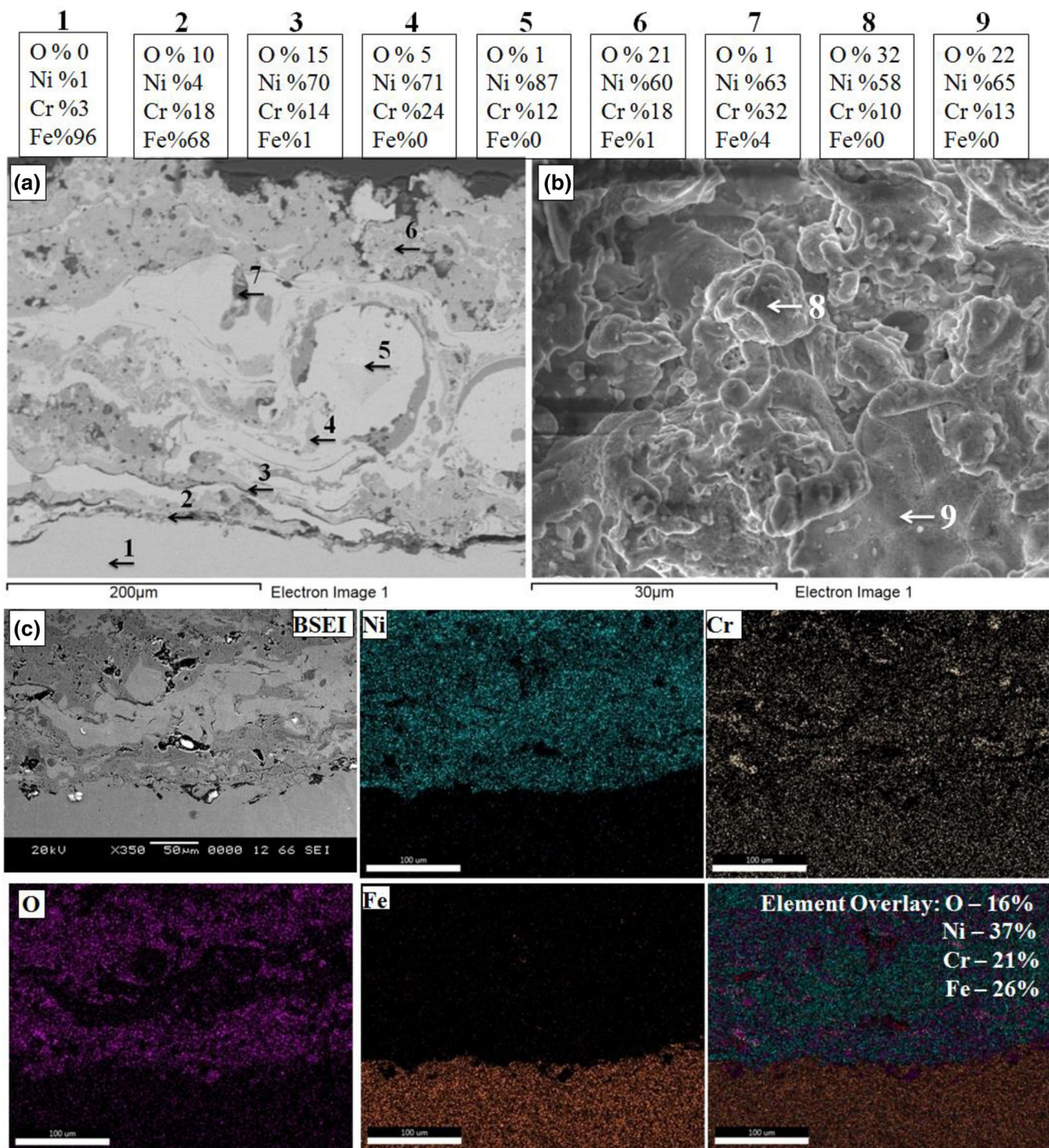
1	2	3	4	5	6	7	8	9
O % 0 Ni %1 Cr %3 Fe%96	O % 10 Ni %4 Cr %18 Fe%68	O % 15 Ni %70 Cr %14 Fe%1	O % 5 Ni %71 Cr %24 Fe%0	O % 1 Ni %87 Cr %12 Fe%0	O % 21 Ni %60 Cr %18 Fe%1	O % 1 Ni %63 Cr %32 Fe%4	O % 32 Ni %58 Cr %10 Fe%0	O % 22 Ni %65 Cr %13 Fe%0

Fig. 8 NiCr partially oxidized coating demonstrating (a, b, and c) similar to Fig. 7

Micro-hardness and Density

The micro-hardness, porosity, and density of a coating are often used to determine its quality. These properties influence the erosion behavior of the coatings (Ref 10). Micro-hardness value was measured on the coatings and substrate at the cross-section (Fig. 9). The micro-hardness values are slightly increased near the coating-substrate interface, which was due to alumina grit blasting prior to the coating. The considerable variation of micro-hardness values throughout the cross-section was due to different oxide phases. The average micro-hardness value of NiCrBSiFe was found to be 809 $HV_{0.3}$ with a 20 standard deviation. With NiCrBSiFe coating by plasma-spray, V.
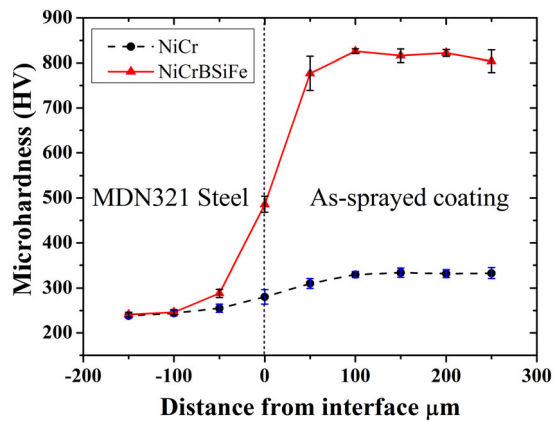
Fig. 9 Variation of micro-hardness values along the substrate and partially oxidized as-sprayed coatings

Higuera Hidalgo et al. (Ref 34) reported lower micro-hardness values. J.M. Miguel et al. (Ref 35) similarly found decreased micro-hardness values with plasma-spray NiCrBSi coating. Thus, the greater micro-hardness values in this investigation are the result of partial oxidation. The average micro-hardness value of NiCr partially oxidized coating was found to be 326 $HV_{0.3}$ with a 9 standard deviation. Micro-hardness of any coating changes with the porosity and density (Ref 36). Porosity less than 1.5% with considerable density represents the quality of the coatings. The average densities of NiCrBSiFe and NiCr coatings are calculated as 5.47 and 5.27 g/cc, respectively.

Erosion Studies

It is imperative to study the erosive wear behavior at elevated temperature as it broadens the applications in the industries and aerospace. Figure 10 differentiates the average volumetric erosion loss of NiCrBSiFe and NiCr partially oxidized coatings response to temperature and impact angles.

Erosion Mechanism of Partially Oxidized NiCrBSiFe Coating

Partially oxidized NiCrBSiFe coating changes its mode of erosion with temperature. It starts with a mixed-mode of erosion from RT to 400°C and is transformed to the ductile mode from 600 to 800°C. Volumetric erosion loss was increased up to 400°C and then reduced due to the formation of $NiCr_2O_4$, Fe_2SiO_4, and $Ni_2B_2O_5$ spinal oxide phases on the surface to resist erosion (Fig. 11). At room temperature, the surface morphology of the eroded sample with a 30° impact angle depicts surface cracks, and the chipping of material from the surface demonstrates a brittle mode of erosion (Fig. 13). Raised lips, strain hardened lips, and deformed surface at 90° impact angle confirm the ductile mode of erosion. Hence, NiCrBSiFe coating exhibits a mixed-mode of erosion at room temperature. N. Krishnamurthy et al. [37] described mixed-mode of failure where ductile and brittle behavior of erosion occurs. As per mixed-mode of erosion, erosive wear at low impact angle is due to micro-cutting and ploughing (Ref 38, 39). Formation of lips, strain hardening of lips, and then a ductile failure of these lips occurs at high impact angle, and maximum erosion occurs between 45 to 60° impact angles.

As the test temperature increases, the partially oxidized region in NiCrBSiFe coating shows ductile nature while the oxide region shows brittle nature. In general, the behavior of the coating exhibits ductile nature and correspondingly produces the oxide layer as the coating is rich in a partially oxidized region. As a result, NiCrBSiFe coating exhibits a mixed-mode of erosion up to 400°C followed by ductile mode of erosion due to a drastic change
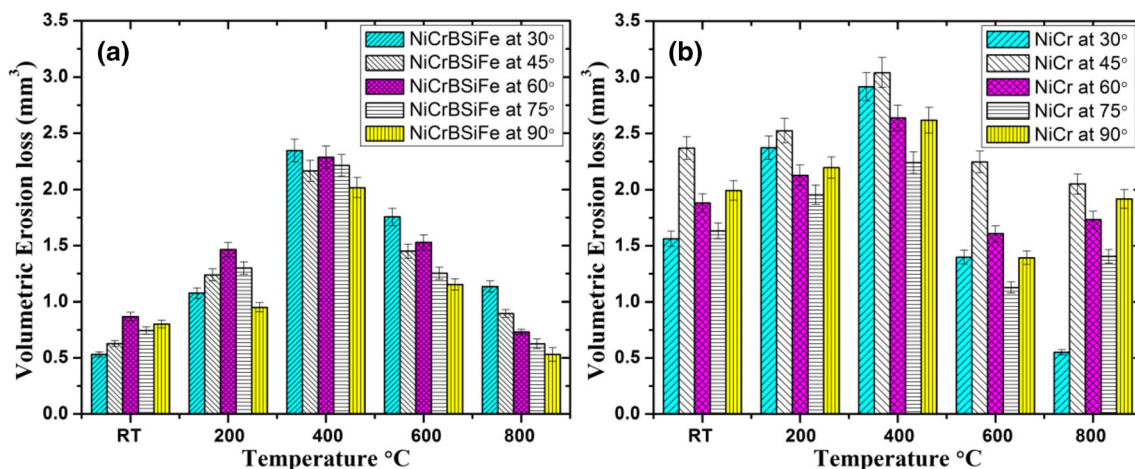

Fig. 10 Variation of volumetric erosion loss of partially oxidized coating (a) NiCrBSiFe and (b) NiCr at different temperatures and impact angles
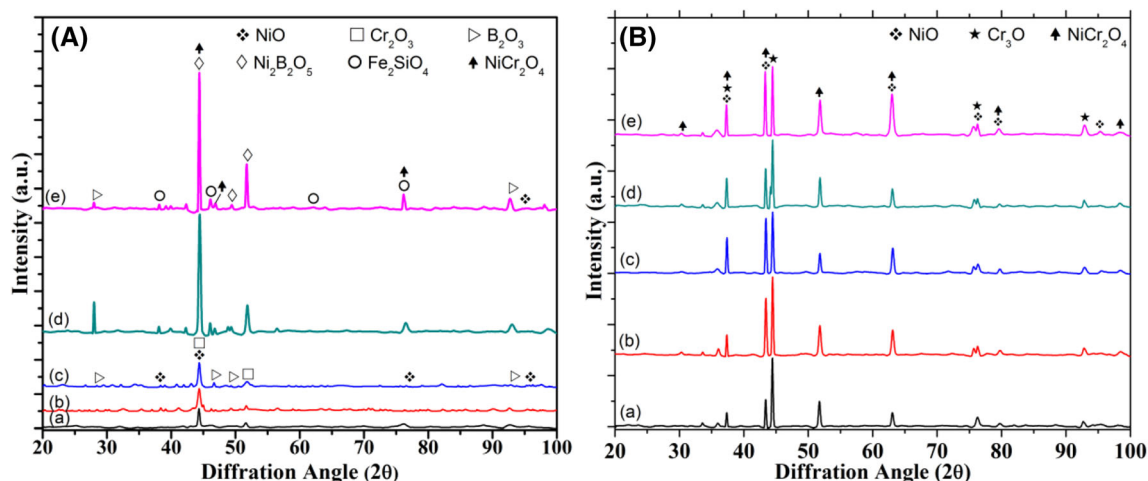
Fig. 11 Eroded samples XRD at (a) RT (b) 200°C (c) 400°C (d) 600°C and (e) 800°C of (A) NiCrBSiFe and (B) NiCr partially oxidized coatings

in the hardness of the partially oxidized region. Moreover, during the erosion test at elevated temperatures, oxidation of surfaces will occur when the specimen is placed inside the heating chamber for 20 minutes, and then the oxidized surface will be eroded (Ref 15, 34). XRD patterns of the eroded surfaces illustrate no significant intensity peaks of the oxide phase present between RT to 400°C to resist the erosion. Fig. 13 also depicts severe erosion loss at RT due to surface cracks, chipping of material from the eroded surface, raised lips, and strain hardened lips. The severity of erosion loss continued up to 400°C because there are no protective oxides formed on the surfaces during erosion. As a result, volumetric erosion loss increased continuously up to 400°C. Even though maximum erosion occurred at a 30° impact angle with 400°C, mixed-mode of erosion exists because the mode of erosion is transforming from mixed mode to ductile mode where two modes of erosion occur. However, between 600 and 800°C, the surface hardness of the coating drastically reduced, which leads to a ductile mode of erosion (Ref 40). Volumetric erosion loss was reduced above 600°C due to the presence of the oxide layer and the embedment of alumina particles into the surface. The presence of $NiCr_2O_4$, Fe_2SiO_4, and $Ni_2B_2O_5$ spinal oxide phases at 600 and 800°C were contributing to improving the erosion resistance (Fig. 10A). The embedded alumina particles act as a shielding effect on the surface to minimize further loss of material. Fig. 12a depicts the series of alumina particles that penetrated NiCrBSiFe coating at 800°C and made white wrinkles on the surface. These white wrinkles were not present in NiCr coating at elevated temperatures (Fig. 12b). Moreover, at higher impact angles, surface hardening due to continuous impact decreases the erosion rate. S. Sharma (Ref 41) studied erosion behavior of flame sprayed NiCrFeSiB coating at different impact angles and reported that the erosion rate

decreased with increased impact angle in a ductile material. At a lower impact angle, erosion occurs by cutting mechanism, whereas at a higher impact angle by the detachment of severely strained debris from the surface.

In NiCrBSiFe coating at 600 and 800°C, volumetric erosion loss at 30° impact angle is greater than the volumetric erosion loss at 90°, which is the characteristic behavior of ductile mode of erosion. Splats boundary strengthening and hardness reduction of oxidized splats at high-temperature results in ploughing and micro cracks at a 30° impact angle. Due to continuous impact at 90°, the eroded surface will be deformed plastically and reduce the erosion loss. Higuera et al. (Ref 34) used NiCrBSiFe coating developed by plasma spray process to study erosion wear behavior of the coating. He reported that the same brittle mode of erosion is taking place in the coating at room temperature and 800°C. As a result, erosion was not controlled even at high temperatures. As the mode of erosion is changing with temperature, it is easy to control the erosion rate in a partially oxidized coating. (Fig. 14)

Erosion Mechanism of Partially Oxidized NiCr Coating

In partially oxidized NiCr coating, volumetric erosion loss increases up to 400°C due to change of coating hardness and then reduced due to oxide phases contributing to improving the erosion resistance (Fig. 11B). The coating exhibits maximum volumetric erosion loss at a 45° impact angle at all temperatures. Fig. 14 depicts micro-cutting and ploughing at 30° impact angle, and raised lips, impact crater and strain hardened phases at 90° impact angle, which demonstrates a mixed-mode of erosion. Even though oxide phases like NiO, Cr_3O, and $NiCr_2O_4$ contributed to resist the erosion at high temperature, could not able to change the mode of erosion. Due to high adhesive strength
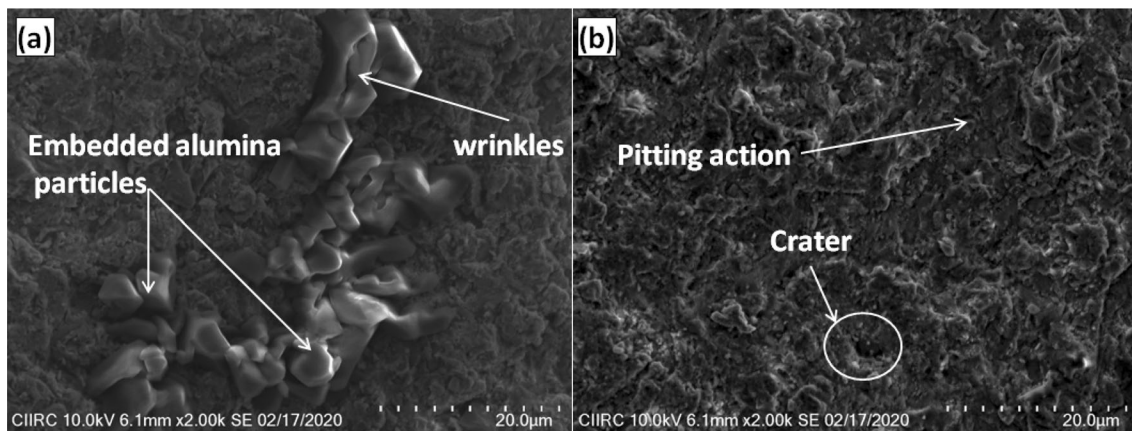
Fig. 12 SEM of eroded surface morphology at 800 °C with 90° impact angle (a) NiCrBSiFe (b) NiCr partially oxidized coatings

between coating and substrate than the cohesive strength between the splats causes the maximum erosive wear at 45° impact angle, where impact force will be equally divided into horizontal and vertical force. In Fig. 14 (f), increased $O_2\%$ and Al% confirmed oxide phases and embedded alumina particles act as a shielding effect for the erosion in NiCr coating. Roy et al. (Ref 42) reported the erosion rate of NiCr alloy increases continuously from RT to 800°C. In partially oxidized NiCr coating, erosion loss decreases from 600 to 800°C, and this cause is because of partial oxidation.

3D Optical Profilometer Studies

Volumetric erosion loss was also analyzed by computer-generated three-dimensional profile pattern through the non-contact type optical profilometer. The image measurements were taken with a 4.98 × 3.74 mm field view on the effective magnification of 5×. The field view had been taken such that the erosion scar is always within the analyzed area. The volumetric erosion loss (V) was estimated by using equation $V = (2\pi\, a \times b \times c)/3$. Where a and b were the lengths (mm) of the major and minor axis of the ellipse at the highest step and c is erosion depth in mm, respectively. The erosion scar at 30° impact angle follows the elliptical shape and its major axis decreases as increasing the angle of impact and becomes equal to the minor axis at 90° impact angle (Fig. 15). The volumetric erosion loss was determined using a 3D optical profilometer correlated with experimental values of both the coatings.

Comparison of Erosion Behavior of Coatings

Partially oxidized NiCrBSiFe coating shows better erosion resistance than partially oxidized NiCr coating. Erosion loss of NiCr was more than two times comparing with

erosion loss of NiCrBSiFe at RT and 800°C. In NiCr, the sudden reduction of erosion loss at 30° impact angle with 800°C is excluded for the comparison as it may be due to a temporary oxide layer on the surface. In NiCrBSiFe coating between 200 and 600°C, mixed-mode to the ductile mode of erosion transition takes place. As a result, volumetric erosion loss was increased up to 400°C and then started decreasing from 600°C. Due to the mixed mode of erosion in NiCr coating, the volumetric erosion loss was not uniform with increasing temperature. Hence, no considerable difference in the erosion loss was recognized between the coatings from 400 to 600°C.

Conclusions

1. Partially oxidized NiCrBSiFe and NiCr powders were processed by the flame spray process, and coatings were successfully deposited by the plasma spray process on MDN321 steel. Under specified spray parameters, dense coatings with an average thickness of 250 µm have been achieved. The average bond strength of NiCrBSiFe and NiCr partially oxidized coatings were 809 ± 20 $HV_{0.3}$ and 326 ± 9 $HV_{0.3}$, respectively.

2. XRD/SEM of partially oxidized powders proved the thin oxide layer and heat effected layer on the core. The thickness of the oxide layer was varied in NiCr particles based on the diameter of the particle, whereas the uniform thickness of the oxide layer was in NiCrBSiFe particles. These results lead NiCr coating is rich in the oxide region while NiCrBSiFe coating is rich in the partially oxidized region.

3. Partially oxidized NiCrBSiFe coating changes its mode of erosion with the temperature. It exhibited a mixed-mode of erosion from room temperature to 400°C and transformed to the ductile mode of erosion from 600 to 800°C. Volumetric erosion loss was reduced at ductile
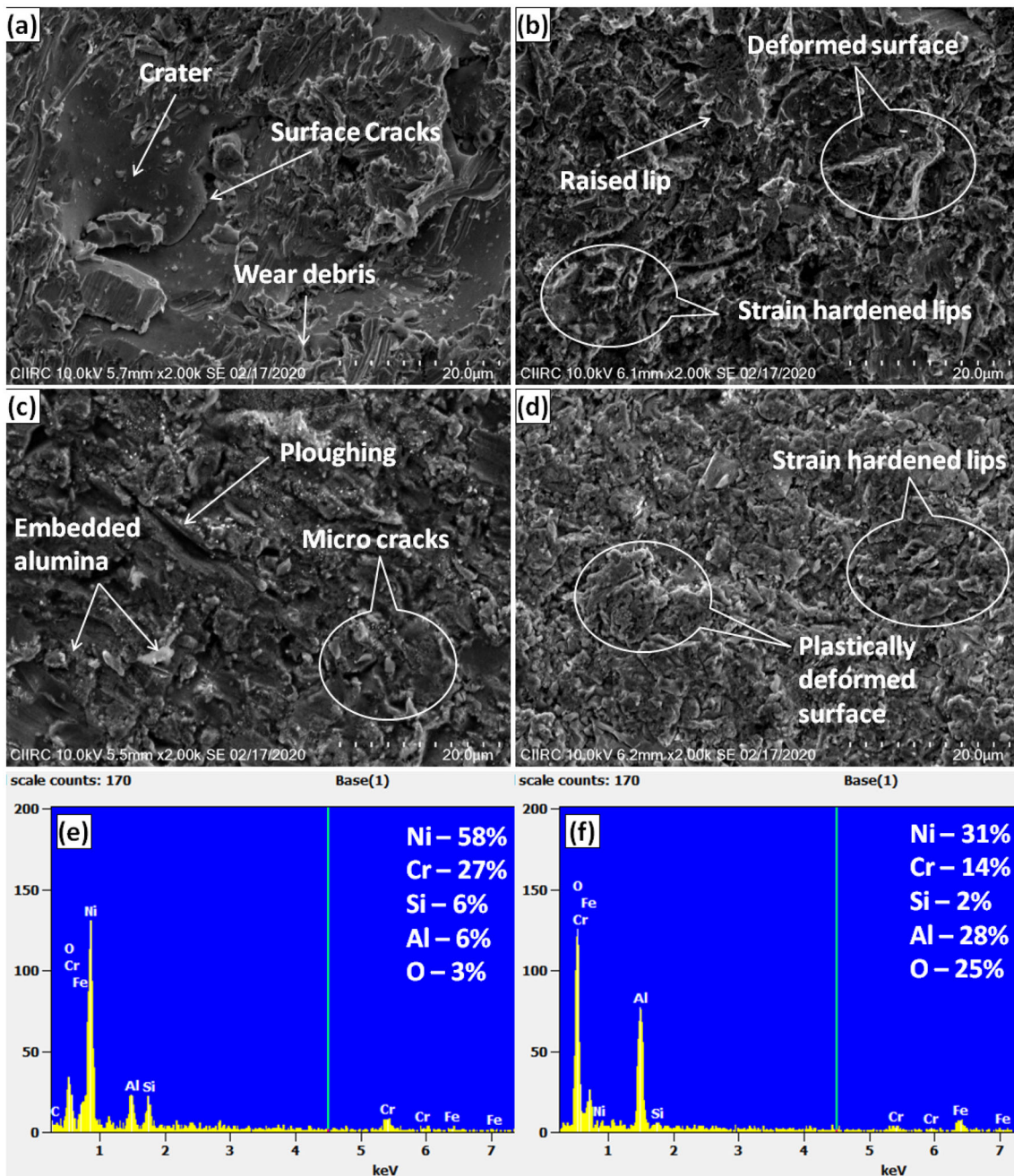
Fig. 13 Eroded surface morphology of NiCrBSiFe partially oxidized coating at room temperature (a, b) and 800°C (c, d) with impact angle 30° (a, c) and 90° (b, d); EDAX surface morphology with a full-length spectrum on the eroded scar at (e) RT with impact angle 30° (f) 800°C with impact angle 90°

mode due to the formation of NiCr$_2$O$_4$, Fe$_2$SiO$_4$, and Ni$_2$B$_2$O$_5$ spinal oxide phases on the surface to resist the erosion.

4. Partially oxidized NiCr coating exhibits maximum volumetric erosion loss at 45° impact angle, and SEM of erosion scar depicts micro-cutting and ploughing at 30° impact angle, and raised lips, impact crater, and strain hardened phases at 90° impact angle, which

demonstrates a mixed-mode of erosion at all temperatures. Even though oxide phases like NiO, Cr$_3$O, and NiCr$_2$O$_4$ contributed to resist the erosion at high temperature, they could not able to transfer the mode of erosion.

5. Partially oxidized NiCrBSiFe coating demonstrates better erosion resistance than partially oxidized NiCr coating. Volumetric erosion loss of NiCr was more
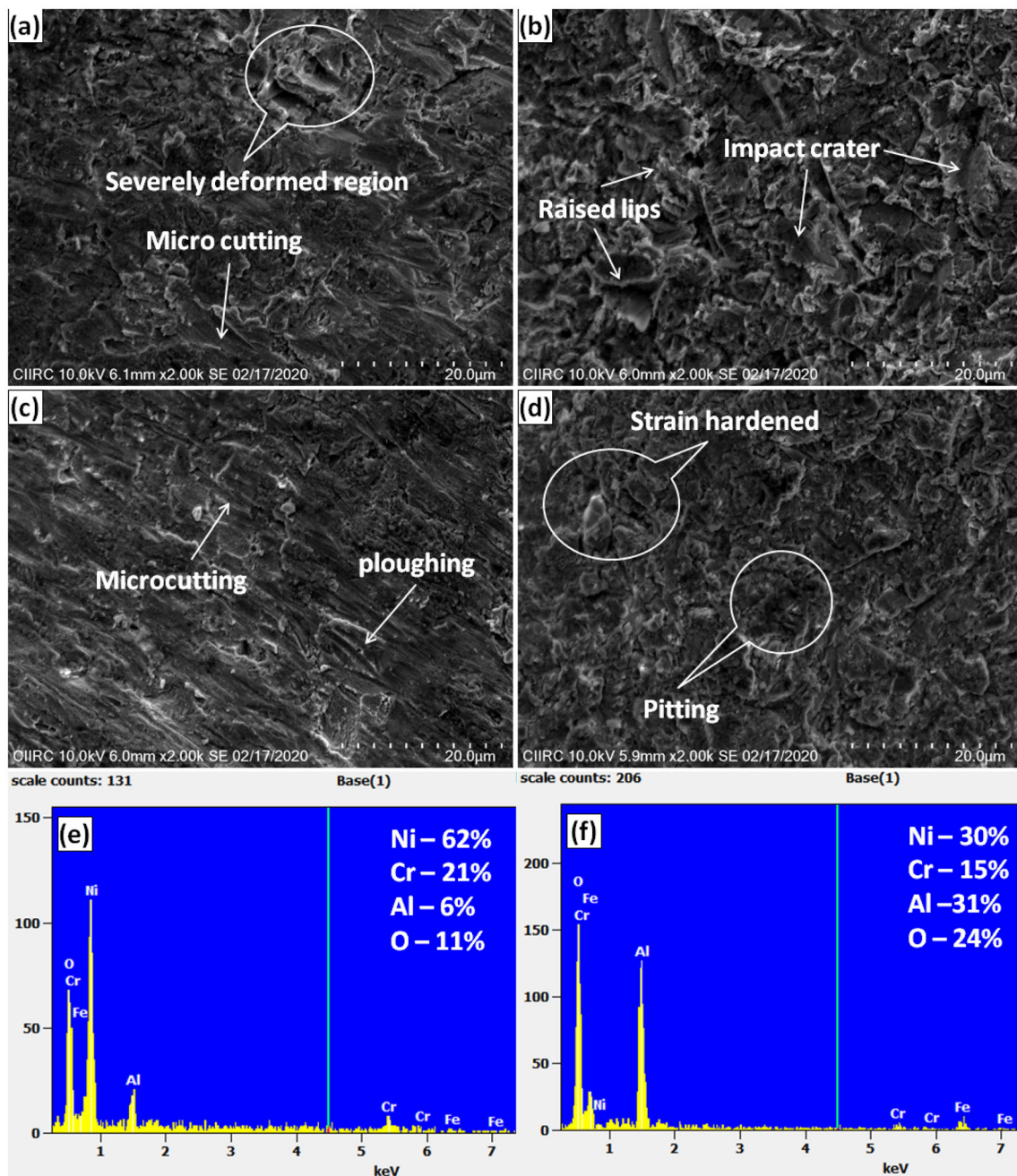
Fig. 14 Eroded surface morphology of NiCr partially oxidized coating demonstrating (a, b, c, d, e, and f) similar to Fig. 13

than two times comparing with volumetric erosion loss of NiCrBSiFe at RT and 800 °C. Mixed-mode to the ductile mode of erosion transition takes place in NiCrBSiFe coating between 200 and 600°C; as a result, no considerable difference in erosion loss was recognized between NiCrBSiFe and NiCr coatings.

6. Volumetric erosion loss was determined using a 3D optical profilometer correlated with experimental values of both the coatings.
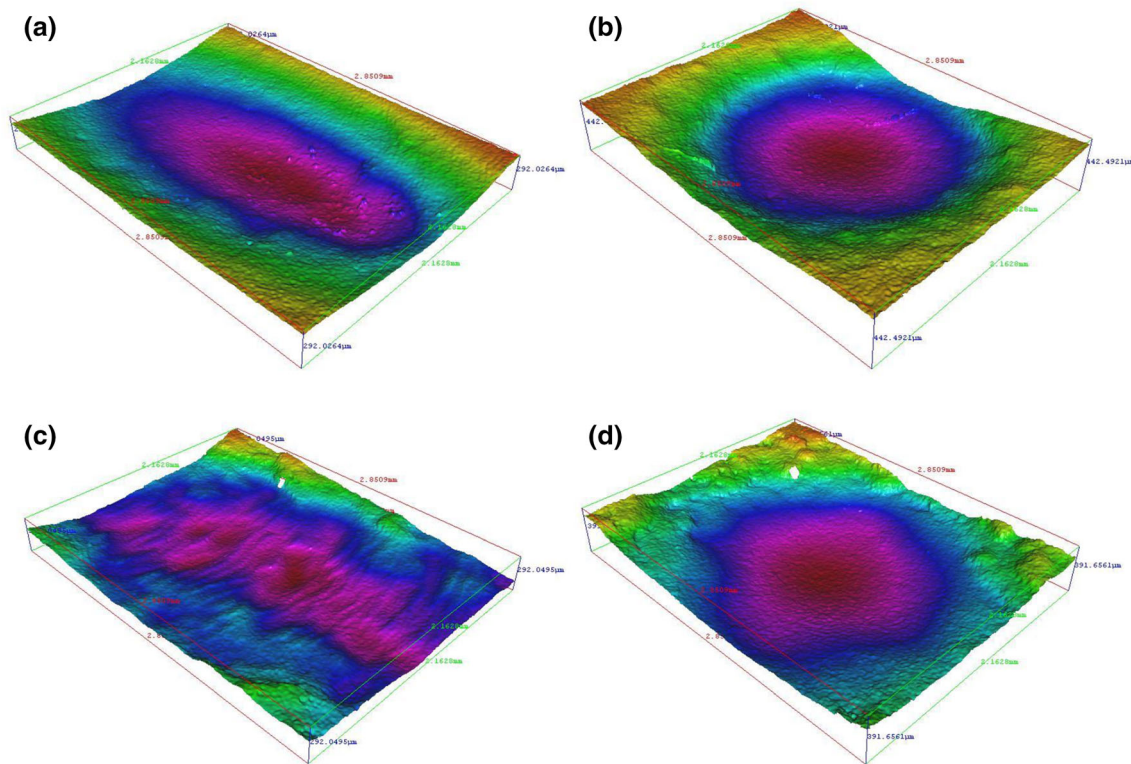
Fig. 15 3D optical profilometer images of NiCrBSiFe (a, b) and NiCr (c, d) coatings at 800 °C with impact angles 30° (a, c) and 90° (b, d)

References

1. S.B. Mishra, K. Chandra, S. Prakash and B. Venkataraman, Erosion performance of coatings produced by shrouded plasma spray process on a Co-based superalloy, *Surf. Coat. Technol.*, 2006, **201**, p 1477–1487.

2. B. Somasundaram, R. Kadoli and M.R. Ramesh, Evaluation of cyclic oxidation and hot corrosion behavior of HVOF-Sprayed WC-Co/NiCrAlY coating, *J. Therm. Spray Technol.*, 2014, **23**(6), p 1000–1008.

3. E. Bousser, L. Martinu and J.E. Klemberg-Sapieha, Solid particle erosion mechanisms of protective coatings for aerospace applications, *Surf. Coat. Technol.*, 2014, **257**, p 165–181.

4. Y.Q. Xiao, L. Yang, Y.C. Zhou, Y.G. Wei and N.G. Wang, Dominant parameters affecting the reliability of TBCs on a gas turbine blade during erosion by a particle-laden hot gas stream, *Wear*, 2017, **390–391**, p 166–175.

5. S.B. Mishra, K. Chandra and S. Prakash, Erosion-corrosion performance of NiCrAlY coating produced by plasma spray process in a coal-fired thermal power plant, *Surf. Coat. Technol.*, 2013, **216**, p 23–34.

6. J.B. Cheng, X.B. Liang, Y.X. Chen, Z.H. Wang, and B.S. Xu, High-temperature erosion resistance of FeBSiNb amorphous coatings deposited by arc spraying for boiler applications, *J. Therm. Spray Technol.*, 2013, p 820–827.

7. H.S. Grewal, H. Singh and A. Agrawal, Microstructural and mechanical characterization of thermal sprayed nickel-alumina composite coatings, *Surf. Coat. Technol.*, 2013, **216**, p 78–92.

8. S. Matthews, B. James and M. Hyland, High temperature erosion-oxidation of Cr3C2-NiCr thermal spray coatings under simulated turbine conditions, *Corros. Sci.*, 2013, **70**, p 203–211.

9. Y. Wang, Y. Yang and M.F. Yan, Microstructures, hardness and erosion behavior of thermal sprayed and heat treated NiAl coatings with different ceria, *Wear*, 2007, **263**, p 371–378.

10. I.R.V. Geaman, M.A. Pop and D.L. Motoc, Tribological properties of thermal spray coatings, *Eur. Sci. J.*, 2013, **3**, p 154–159.

11. P. Bagde, S.G. Sapate, R.K. Khatirkar and N. Vashishtha, Friction and abrasive wear behaviour of Al_2O_3-13TiO_2 and Al_2O_3-13TiO_2+Ni graphite coatings, *Tribol. Int.*, 2018, **121**, p 353–372.

12. A. Richter, L.M. Berger, Y.J. Sohn, S. Conze, K. Sempf, and R. Vaßen, Impact of Al_2O_3-40 Wt.% TiO_2 feedstock powder characteristics on the sprayability, microstructure and mechanical properties of plasma sprayed coatings, *J. Eur. Ceram. Soc.*, 2019, **39**(16), p 5391–5402.

13. X. Yang, S. Dong, J. Zeng, X. Zhou, J. Jiang, L. Deng, and X. Cao, Sliding wear characteristics of plasma-sprayed Cr_2O_3 coatings with incorporation of metals and ceramics, *Ceram. Int.*, 2019, p 20243–20250.

14. K.G. Girisha, K.V. Sreenivas Rao, and C. Durga Prasad, Slurry erosion resistance of martenstic stainless steel with plasma sprayed Al_2O_3-40%TiO_2 coatings, *Mater. Today Proc.*, 2018, **5**(2), p 7388–7393.

15. H.S. Nithin, V. Desai and M.R. Ramesh, Elevated temperature solid particle erosion performance of plasma-sprayed Co-based composite coatings with additions of Al_2O_3 and CeO_2, *J. Mater. Eng. Perform.*, 2017, **26**, p 5251–5261.

16. L. He, Y. Tan, H. Tan, Y. Tu and Z. Zhang, Microstructure and tribological properties of WC-CeO₂/Ni-base alloy composite coatings, *Rare Met. Mater. Eng.*, 2014, **43**(4), p 823–829.

17. M.R. Ramesh, S. Prakash, S.K. Nath, P.K. Sapra and B. Venkataraman, Solid particle erosion of HVOF sprayed WC-Co/NiCrFeSiB coatings, *Wear*, 2010, **269**, p 197–205.

18. Z. Xia, X. Zhang and J. Song, Erosion-resistance of plasma sprayed coatings, *J. Mater. Eng. Perform.*, 1999, **8**(6), p 716–718.

19. K.A. Unocic and B.A. Pint, Oxidation behavior of Co-doped NiCrAl alloys in dry and wet air, *Surf. Coat. Technol.*, 2013, **237**, p 8–15.

20. T. Irisawa and H. Matsumoto, Thermal shock resistance and adhesion strength of plasma-sprayed alumina coating on cast iron, *Thin Solid Films*, 2006, **509**, p 141–144.

21. A.C. Karaoglanli, H. Dikici and Y. Kucuk, Effects of heat treatment on adhesion strength of thermal barrier coating systems, *Eng. Fail. Anal.*, 2013, **32**, p 16–22.

22. N.C. Reddy, B.S.A. Kumar, M.R. Ramesh and P.G. Koppad, Microstructure and adhesion strength of Ni₃Ti coating prepared by mechanical alloying and HVOF, *Phys. Met. Metallogr.*, 2018, **119**(5), p 462–468.

23. T.A. Taylor and P.N. Walsh, Dilatometer studies of NiCrAlY coatings, *Surf. Coat. Technol.*, 2004, **188–189**, p 41–48.

24. S.R. Medabalimi, M. R. Ramesh and R. Kadoli, High-temperature wear and frictional behavior of partially oxidized Al with NiCr composite coating, *Mater. Res. Express.*, IOP Publishing, 2019, **6**(12), p 1–13.

25. J.M. Guilemany, N. Cinca, J. Fernández, and S. Sampath, Erosion, abrasive, and friction wear behavior of iron aluminide coatings sprayed by HVOF, *J. Therm. Spray Technol.*, 2008, p 762–773.

26. M. Doddamani, M. Mathapati and M.R. Ramesh, Microstructure and tribological behavior of plasma sprayed NiCrAlY / WC- Co / Cenosphere / solid lubricants composite coatings, *Surf. Coat. Technol.*, 2018, **354**, p 92–100.

27. M. Ivosevic, R. Knight, S.R. Kalidindi, G.R. Palmese and J.K. Sutter, Solid particle erosion resistance of thermally sprayed functionally graded coatings for polymer matrix composites, *Surf. Coat. Technol.*, 2006, **200**, p 5145–5151.

28. W. Tillmann, L. Hagen, D. Stangier, I.A. Laemmerhirt, D. Biermann, P. Kersting and E. Krebs, Wear behavior of Bio-inspired and technologically structured HVOF sprayed NiCrBSiFe coatings, *Surf. Coat. Technol.*, 2015, **280**, p 16–26.

29. P. Farahpour, H. Edris, M.M. Kheirikhah, and A.H. Mirrahimi, Influence of high velocity oxy-fuel parameters on the corrosion resistance of NiCr coatings, *Proc. Inst. Mech. Eng. Part L: J. Mater. Des. Appl.*, 2013, **227**(4), p 318–335.

30. C. Huang, L. Du, and W. Zhang, Friction and wear characteristics of plasma-sprayed self-lubrication coating with clad powder at elevated temperatures up to 800 °C, *J. Therm. Spray Technol.*, 2014, p 463–469.

31. C. Huang, L. Du and W. Zhang, Effects of solid lubricant content on the microstructure and properties of NiCr/Cr₃C₂-BaF₂·CaF₂ composite coatings, *J. Alloys Compd.*, 2009, **479**, p 777–784.

32. M. Mathapati, M.R. Ramesh and M. Doddamani, High temperature erosion behavior of plasma sprayed NiCrAlY/WC-Co/Cenosphere coating, *Surf. Coat. Technol.*, 2017, **325**, p 98–106.

33. J.J. Tian, S.W. Yao, X.T. Luo, C.X. Li and C.J. Li, An effective approach for creating metallurgical self-bonding in plasma-spraying of NiCr-Mo coating by designing shell-core-structured powders, *Acta. Mater.*, 2016, **110**, p 19–30.

34. V.H. Hidalgo, F.J.B. Varela, A.C. Menéndez and S.P. Martínez, A Comparative study of high-temperature erosion wear of plasma-sprayed NiCrBSiFe and WC-NiCrBSiFe coatings under simulated coal-fired boiler conditions, *Tribol. Int.*, 2001, **34**, p 161–169.

35. J.M. Miguel, J.M. Guilemany and S. Vizcaino, Tribological study of NiCrBSi coating obtained by different processes, *Tribol. Int.*, 2003, **36**, p 181–187.

36. L. Du, C. Huang, W. Zhang, T. Li and W. Liu, Preparation and wear performance of NiCr/Cr₃C₂-NiCr/HBN plasma sprayed composite coating, *Surf. Coat. Technol.*, 2011, **205**, p 3722–3728.

37. N. Krishnamurthy, M.S. Murali, B. Venkataraman and P.G. Mukunda, Characterization and solid particle erosion behavior of plasma sprayed alumina and calcia-stabilized zirconia coatings on Al-6061 substrate, *Wear*, 2012, **274–275**, p 15–27.

38. H.S. Sidhu, B.S. Sidhu and S. Prakash, Comparative characteristic and erosion behavior of NiCr coatings deposited by various high-velocity oxyfuel spray processes, *J. Mater. Eng. Perform.*, 2006, **15**(6), p 699–704.

39. H. Zhang, X. Dong and S. Chen, Solid particle erosion-wear behaviour of Cr₃C₂-NiCr coating on Ni-based superalloy, *Adv. Mech. Eng.*, 2017, **9**(3), p 1–9.

40. J.K.N. Murthy, K. Satya Prasad, K. Gopinath, and B. Venkataraman, Characterisation of HVOF sprayed Cr₃C₂-50(Ni20Cr) coating and the influence of binder properties on solid particle erosion behaviour, *Surf. Coat. Technol.*, 2010, **204**(24), p 3975–3985.

41. S. Sharma, High temperature erosive wear study of NiCrFeSiB flame sprayed coatings, *J. Inst. Eng. Ser. D.*, 2012, **93**(1), p 7–12.

42. M. Roy, K.K. Ray and G. Sundararajan, Erosion-oxidation interaction in Ni and Ni-20Cr alloy, *Metall. Mater. Trans. A: Phys. Metall. Mater. Sci.*, 2001, **32A**, p 1431–1451.